Research Square

Preprints are preliminary reports that have not undergone peer review.
They should not be considered conclusive, used to inform clinical practice,
or referenced by the media as validated information.

Enhancing O-GlcNAcylation Alleviates α-Synuclein Pathology in a Novel Oligodendroglial α-Synuclein Mouse Model of Multiple System Atrophy

Xiao Dong
Department of Neurology, Xiangya Hospital, Central South University
Linlin Wan
Department of Neurology, Xiangya Hospital, Central South University
Sudan Zhu
Department of Neurology, Xiangya Hospital, Central South University
Xinrong Yuan
Department of Neurology, Xiangya Hospital, Central South University
Zhao Chen
Department of Neurology, Xiangya Hospital, Central South University
Chunrong Wang
Department of Neurology, Xiangya Hospital, Central South University
Linliu Peng
Department of Neurology, Xiangya Hospital, Central South University
Riwei Ouyang
Department of Neurology, Xiangya Hospital, Central South University
Daji Chen
Department of Neurology, Xiangya Hospital, Central South University
Xiaokang Wu
Department of Neurology, Xiangya Hospital, Central South University
Yuteng He
Department of Neurology, Xiangya Hospital, Central South University
Rong Qiu
School of Computer Science and Engineering, Central South University, Changsha
Beisha Tang
Department of Neurology, Xiangya Hospital, Central South University
Hong Jiang
jianghong73868@csu.edu.cn

Department of Neurology, Xiangya Hospital, Central South University

Article

Keywords:

Posted Date: November 24th, 2026

DOI: https://doi.org/10.21203/rs.3.rs-11687234/v1

License: This work is licensed under a Creative Commons Attribution 4.0 International License.
Read Full License

Additional Declarations: No competing interests reported.

Abstract

Background

Multiple system atrophy (MSA) is characterized by oligodendroglial α-synuclein (α-syn) accumulation, but the contribution of O-linked β-*N*-acetylglucosamine (O-GlcNAc) dysregulation to MSA pathology remains unclear.

Objective

To establish a novel oligodendroglial α-syn mouse model and determine whether modulating O-GlcNAcylation affects MSA-like pathology.

Methods

A knock-in (KI) mouse expressing human *SNCA* under the control of the mouse *Plp1* promoter was generated using CRISPR/Cas9. Neuropathological, behavioral, autonomic, and structural abnormalities were characterized longitudinally. Brain O-GlcNAc homeostasis was assessed across disease stages, followed by O-GlcNAc proteomic profiling. KI mice were treated with the O-GlcNAcase inhibitor Thiamet-G (TMG) for 8 weeks. The effects of bidirectional O-GlcNAc modulation were further examined in two TPPP-enhanced oligodendroglial α-syn cell models.

Results

KI mice developed oligodendroglial pS129-α-syn-positive inclusion-like structures, insoluble α-syn species, progressive nigrostriatal and Purkinje cell abnormalities, impaired motor coordination, early blood-pressure alterations, and selective brain atrophy. Global O-GlcNAcylation and O-GlcNAc transferase expression were reduced in the cerebellum and basal ganglia at 9 months, while O-GlcNAc proteomics revealed extensive remodeling of metabolic, proteostatic, and synaptic pathways. TMG increased brain O-GlcNAcylation, improved rotarod and balance-beam performance, reduced pS129-α-syn and glial reactivity, and partially restored tyrosine hydroxylase immunoreactivity. In oligodendroglial cell models, TMG reduced protein aggregation and improved cell viability, whereas the O-GlcNAc transferase inhibitor OSMI-1 produced the opposite effects. No detectable direct O-GlcNAcylation of α-syn was observed.

Conclusions

This KI model recapitulates multiple features of MSA and reveals stage-dependent disruption of brain O-GlcNAc homeostasis. Pharmacological enhancement of O-GlcNAcylation attenuates α-syn-associated

pathological and functional abnormalities, supporting the OGT-OGA axis as a potential therapeutic target for MSA.

Introduction

Multiple system atrophy (MSA) is a rare, rapidly progressive neurodegenerative disorder clinically characterized by variable combinations of autonomic failure, poorly levodopa-responsive parkinsonism, and cerebellar ataxia[1–3]. MSA has a median survival of only 6–10 years from symptom onset, during which worsening autonomic and motor dysfunction leads to severe disability and a substantial decline in quality of life[4–7]. No effective disease-modifying therapy has yet been shown to slow MSA progression, and clinical management remains largely symptomatic, placing a substantial burden on affected individuals, their families, and society[8, 9].

The neuropathological hallmark of MSA is the formation of glial cytoplasmic inclusions (GCIs) within oligodendrocytes, with α-synuclein (α-syn) as their major protein component[10, 11]. Under pathological conditions, α-syn misfolds and progressively assembles into β-sheet-rich oligomers and amyloid fibrils[12]. Abnormal α-syn accumulation is closely associated with endoplasmic reticulum stress, mitochondrial and redox dyshomeostasis, and impaired protein clearance. These processes may reinforce one another, ultimately disrupting oligodendroglial homeostasis and driving neurodegeneration[13–17].

O-linked N-acetylglucosamine (O-GlcNAc) is a dynamic and reversible post-translational modification that is added by O-GlcNAc transferase (OGT) and removed by O-GlcNAcase (OGA)[18, 19]. O-GlcNAcylation broadly regulates cellular metabolism, stress responses, and proteostasis[20, 21]. Accumulating evidence indicates that global cellular O-GlcNAc homeostasis is disrupted in neurodegenerative diseases[22, 23]. Reduced brain O-GlcNAcylation has been reported in patients with Alzheimer's disease (AD)[24, 25] and in mouse models of Parkinson's disease (PD)[26, 27]. Moreover, studies in animal models of AD and PD have shown that increasing brain O-GlcNAcylation can reduce α-syn aggregate formation and neuroinflammation and attenuate neuronal loss[25–29].

Although MSA and PD are both synucleinopathies, PD is characterized predominantly by neuronal α-syn accumulation, whereas the defining pathology of MSA is the formation of GCIs in oligodendrocytes[30, 31]. It remains unclear whether α-syn pathology disrupts O-GlcNAc homeostasis in MSA, whether increasing O-GlcNAcylation can alleviate oligodendroglial α-syn pathology, and which mechanisms may mediate such effects. In this study, we first established and characterized a novel CRISPR/Cas9-mediated mouse model of MSA. We then used this model to define changes in O-GlcNAcylation during MSA-like disease progression and to determine whether increasing O-GlcNAcylation attenuates α-syn pathology and neurological dysfunction. Finally, O-GlcNAc proteomics was used to identify differentially modified proteins and associated biological pathways, thereby providing experimental evidence for the role and potential therapeutic relevance of O-GlcNAc homeostasis in MSA.

Materials and methods

Animals and ethics statement

Male mice on a C57BL/6J background were used. Animals were housed under specific pathogen-free conditions at 22 ± 2°C and 50–60% relative humidity on a 12h light/dark cycle, with ad libitum access to food and water. All animal procedures were conducted in accordance with the Regulations for the Administration of Affairs Concerning Experimental Animals in China and were approved by the Animal Welfare and Ethics Committee of Central South University.

Generation of the oligodendrocyte-directed hSNCA knock-in mouse model

An oligodendrocyte-directed *hSNCA* knock-in mouse model was generated by CRISPR-Cas9-mediated insertion of an *mPlp1-hSNCA* expression cassette into the mouse H11 safe-harbor locus. The cassette contained the human SNCA-205 transcript under the control of mouse *Plp1* regulatory elements, comprising approximately 2.4kb upstream of the transcription start site, exon 1, intron 1, and the first 37 bp of exon2. The Plp1 initiation codon was changed from ATG to GAG to prevent unintended translation from the Plp1 sequence. Cas9 protein, sgRNA, and the donor vector were co-delivered into fertilized C57BL/6J oocytes, which were subsequently transferred into pseudopregnant females. Founder mice were screened by PCR across the targeted locus and confirmed by Sanger sequencing. Positive F0 founders were backcrossed with C57BL/6J mice to establish a germline-transmissible line.

Genotyping

Genomic DNA was extracted from tail biopsies. The wild-type H11 allele and the 5' junction between the inserted cassette and the H11 locus were amplified by PCR and analyzed by agarose gel electrophoresis. The expected amplicons were 825bp for the wild-type allele and 390 bp for the knock-in allele. Mice displaying only the 825bp band were classified as wild type (WT), those displaying both bands as heterozygous knock-in (KI), and those displaying only the 390-bp band as homozygous knock-in. PCR products were separated on 1% agarose gels and visualized using a gel documentation system. Primer sequences are provided in Supplementary Table 1.

O-GlcNAc-modified proteomic analysis

Brain tissues from 12-month-old WT and MSA-KI mice (n = 4 per group) were subjected to O-GlcNAc-modified proteomic analysis by Shanghai Applied Protein Technology Co., Ltd. Proteins were extracted, reduced, alkylated, and digested with trypsin. O-GlcNAc-modified peptides were enriched using anti-GlcNAc-S/T antibody-conjugated magnetic beads and separated using a nanoElute ultra-high-performance liquid chromatography system (Bruker Daltonics). Peptides were analyzed using a timsTOF Pro mass spectrometer (Bruker Daltonics) operated in parallel accumulation-serial fragmentation (PASEF) mode. The resulting data were searched using PEAKS with a peptide-spectrum match false

discovery rate of ≤ 1%. Differentially modified peptides were defined by a fold change > 2.0 or < 0.5 and $P < 0.05$.

Experimental groups and TMG administration

Eight-month-old male WT mice (n = 10) and mPlp1-hSNCA KI mice (n = 20) were used for the intervention study. KI mice were randomly assigned to the KI mice treated with PBS and KI mice treated with TMG groups (n = 10 per group), whereas WT mice received an equivalent volume of PBS. TMG was administered intraperitoneally at 35mg/kg once every 3 days for 8 weeks. Control mice received PBS using the same route and schedule. Behavioral assessments were conducted before treatment and after 4 and 8 weeks of treatment.

Behavioral and autonomic assessments

Behavioral tests were conducted at approximately the same time each afternoon in a quiet, controlled environment Motor function was assessed using the balance-beam, rotarod, hanging test and grip-strength tests. For the balance-beam test, mice traversed a 100-cm-long, 0.5-cm-wide beam positioned 50cm above the floor, and traversal time was recorded. For the rotarod test, mice were tested at 40 rpm for a maximum of 400s, and latency to fall was recorded. For the hanging test, mice were allowed to grasp a horizontal wire grid, and the latency to fall was recorded. For the grip-strength test, mice were allowed to grasp the bar of a grip-strength meter with their forepaws and were gently pulled backward by the tail until they released the bar; the peak force was recorded. Each test was repeated three times, and the mean value was used for analysis.

Blood pressure was measured using a non-invasive tail-cuff system. Mice were placed in an opaque restrainer, and the sensor was positioned at the base of the tail. After the mice had become calm, five consecutive measurements were obtained, and the mean value was used for analysis.

Magnetic resonance imaging

Male WT and KI mice aged 4, 8, and 12 months underwent brain MRI using a 7.0-T Siemens MAGNETOM Terra scanner equipped with [insert animal coil]. Anesthesia was induced with 2% isoflurane and maintained with 1% isoflurane during image acquisition. Sagittal and coronal T2-weighted images were acquired using the following parameters: repetition time, 3200ms; echo time, 79ms; echo-train length, 11; field of view, 25×25mm; voxel size, 1.0×0.0868×0.0868mm; slice thickness, 1mm; and 18 slices. Images were segmented using SPM12 and RESTplus in MATLAB. Whole-brain and predefined region-of-interest volumes were subsequently extracted.

Tissue collection and processing

Mice were deeply anesthetized with 1% pentobarbital and transcardially perfused with ice-cold PBS. Brains were removed and sagittally divided into two hemispheres. One hemisphere was fixed in 4% paraformaldehyde, dehydrated through a graded ethanol series, cleared in xylene, embedded in paraffin, and cut into 4-μm sagittal sections for histological analysis. The other hemisphere was snap-frozen in liquid nitrogen and stored at -80°C for protein extraction.

Immunofluorescence staining

Sagittal paraffin sections (4μm) from matched anatomical levels were used for immunofluorescence staining. Sections were deparaffinized, rehydrated, and subjected to heat-induced antigen retrieval in citrate buffer using a microwave oven. After cooling to room temperature and washing with PBS, sections were blocked for 1h at room temperature in buffer containing 5% normal goat serum and incubated with primary antibodies overnight at 4°C. The following day, sections were washed with PBS and incubated with the appropriate fluorophore-conjugated secondary antibodies for 2h in the dark. Nuclei were counterstained with DAPI for 10 min, and sections were mounted using an antifade mounting medium. Full antibody information, including host species, supplier, catalog number, and dilution, is provided in Supplementary Table 2.

Cell culture, generation of a stable cell line, and establishment of oligodendroglial α-syn models

The human oligodendroglial cell line MO3.13 was maintained in DMEM/F12 supplemented with 10% fetal bovine serum and 1% penicillin–streptomycin at 37°C in a humidified atmosphere containing 5%CO_2. Cells were passaged or transfected at approximately 70–80% confluence.

To generate MO3.13 cells stably expressing human α-syn, cells were transduced with a recombinant lentivirus carrying the human SNCA coding sequence and a puromycin-resistance cassette. An empty-vector lentivirus served as the control. At 16h after transduction, the medium was replaced, and puromycin 5μg/mL was added after transduction. Selection medium was replaced every 2–3 days until non-transduced control cells had died and the transduced population exhibited stable growth. Stable α-syn expression was confirmed by western blotting.

Two oligodendroglial α-syn pathology models were used. In the transient model, MO3.13 cells were co-transfected with human SNCA and TPPP/p25α expression plasmids. In the stable model, a TPPP/p25α expression plasmid was transiently introduced into MO3.13 cells stably expressing human α-syn. Corresponding control cells received equivalent amounts of empty vector. Schematics of the expression constructs are provided in Supplementary Fig. 1.

Cell transfection and pharmacological treatment

Plasmid transfection was performed using Lipofectamine 3000 according to the manufacturer's instructions. Six hours after transfection, the medium was replaced, and cells were treated with

25μmol/L TMG or 35μmol/L OSMI-1 for 36h.

Thioflavin T assay

Following the indicated treatments, cells were seeded into black 96-well plates at 3,000 cells per well and cultured for an additional 18h to allow attachment without substantial overlap. Before measurement, cells were gently washed with PBS to remove colored components of the culture medium. Each well then received 100μL of Thioflavin T(ThT) working solution at a final concentration of 25μmol/L. Plates were incubated at 37°C for 1h in the dark, and fluorescence was measured using a multimode plate reader at excitation and emission wavelengths of 450 and 480nm, respectively.

Cell viability assay

Following the indicated treatments, cells were seeded into clear 96-well plates at 3,000 cells per well and cultured for an additional 18h. Control, treatment, and cell-free blank wells were included. Cells were gently washed with PBS, after which fresh culture medium containing 10μL of Cell Counting Kit-8 reagent per well was added. Plates were incubated at 37°C for 1h in the dark, and absorbance at 450nm was measured using a multimode plate reader. Values were corrected by subtraction of the cell-free blank.

Western blotting

Brain tissues or cultured cells were lysed in ice-cold RIPA buffer supplemented with protease and phosphatase inhibitors. Tissue samples were homogenized on ice, whereas cells were washed with ice-cold PBS and lysed for 30min on ice. Lysates were centrifuged at 12,000×g for 15min at 4°C, and the supernatants were collected. Protein concentrations were determined using a BCA assay. Equal amounts of protein were mixed with sample buffer and heated at 95°C for 5-10min. Proteins were separated on 12% SDS-PAGE gels and transferred to PVDF membranes. Membranes were blocked for 1h at room temperature in TBST containing 5% non-fat milk and incubated with primary antibodies overnight at 4°C. After three washes with TBST, membranes were incubated with the appropriate HRP-conjugated secondary antibodies for 2h at room temperature. Signals were developed using an enhanced chemiluminescence substrate and captured with a chemiluminescence imaging system.

Statistical analysis

Statistical analyses and data visualization were performed using R version 4.2.1 and GraphPad Prism version 9.5.1. Comparisons between two groups were performed using Student’s t-test, whereas comparisons among multiple groups were performed using one-way ANOVA. GO annotation and enrichment analysis were performed using Blast2GO, and KEGG pathway analysis was conducted by mapping the identified proteins to the KEGG database. $P < 0.05$ was considered statistically significant.

Results

Generation and characterization of a novel mouse model with oligodendroglial expression of human α-synuclein

We generated a KI mouse model expressing human *SNCA* under the control of the mouse *Plp1* promoter using CRISPR/Cas9 technology (Fig. 1A). Successful integration of the target sequence was confirmed by PCR genotyping and Sanger sequencing (Supplementary Fig. 2A, B).

Human α-syn was readily detected in the cerebellum and brainstem of KI mice at 2 months of age but was absent in WT mice (Fig. 1B). KI mice also showed increased pS129-α-syn in the cerebellum and basal ganglia without a significant change in total α-syn (Fig. 1C). Moreover, Triton X-100-insoluble fractions from 8-month-old KI mice contained enriched high-molecular-weight pS129-α-syn species, consistent with insoluble α-syn accumulation (Supplementary Fig. 2C). In 8-month-old KI mice, pS129-α-syn formed dense punctate or inclusion-like cytoplasmic structures within CNPase-positive regions and around OLIG2-positive nuclei, supporting its accumulation in oligodendrocytes (Fig. 1D, E)

Age-dependent neuropathological changes were subsequently examined. TH immunoreactivity was preserved at 2–6 months but decreased significantly in KI mice at 8 and 12 months (Fig. 1F, G). Calbindin-D28K expression and the number of Calbindin-D28K-positive Purkinje cells were significantly reduced at 12 months, indicating later-onset Purkinje cell pathology (Fig. 1H, I). No extensive cerebellar demyelination was detected by Luxol fast blue staining (Supplementary Fig. 2E).

Longitudinal behavioral testing revealed no significant difference in hanging latency between genotypes (Fig. 1J). KI mice showed reduced rotarod latency at 12 months and prolonged balance-beam traversal time at 8 and 12 months, indicating progressive impairment of motor coordination and balance (Fig. 1K, L). KI mice also exhibited signs of cardiovascular autonomic dysfunction. Six-month-old male KI mice also exhibited lower systolic blood pressure than WT mice, whereas diastolic and mean arterial pressures showed nonsignificant downward trends (Supplementary Fig. 2D). Structural MRI at 8 months revealed reduced volumes of the hippocampus, striatum, midbrain, substantia nigra, and pons in KI mice (Fig. 1M).

Collectively, this KI model developed oligodendroglial α-syn pathology followed by progressive nigrostriatal and cerebellar abnormalities, motor dysfunction, early blood-pressure changes, and selective brain atrophy, recapitulating multiple features of MSA.

Brain O-GlcNAcylation and OGT expression are reduced in 9-month-old KI mice

To determine whether human α-syn expression alters brain O-GlcNAc homeostasis, global protein O-GlcNAcylation was measured using the RL2 antibody in the cerebellum and basal ganglia of WT and KI mice at different ages. No significant genotype-dependent differences were observed at 6, 8, 12, or 20 months. At 9 months, however, RL2 signals were significantly reduced in both regions in KI mice compared with age-matched WT mice (Fig. 2A). This reduction was therefore age-dependent and most evident at 9 months, rather than progressive with age. RL2 immunofluorescence further confirmed reduced signals in the cerebellum and basal ganglia (Fig. 2B). Histological analyses supported these

findings. RL2 immunohistochemistry showed weaker O-GlcNAc immunoreactivity and a lower proportion of RL2-positive cells in the cerebellum of 9-month-old KI mice (Fig. 2C).

We next examined the enzymes responsible for O-GlcNAc cycling in 9-month-old mice. OGT protein levels were significantly reduced in both the cerebellum and basal ganglia of KI mice, whereas OGA levels were not significantly altered (Fig. 2D). The reduction in global O-GlcNAcylation at this age was therefore associated with decreased OGT expression rather than increased OGA expression. To investigate whether α-syn pathology involved a direct interaction with OGT, we performed co-immunoprecipitation but detected no specific OGT signal in FLAG-α-syn immunoprecipitates (Supplementary Fig. 3).

Collectively, these results demonstrate an age- dependent disruption of O-GlcNAc homeostasis in KI mice. The reduction in brain O-GlcNAcylation at 9 months was accompanied by lower OGT expression, providing a rationale for pharmacologically increasing O-GlcNAcylation.

The O-GlcNAc-modified proteome is extensively remodeled in MSA-KI mice

To characterize the molecular networks associated with altered O-GlcNAcylation, O-GlcNAc-modified peptides were enriched from whole-brain tissue of 12-month-old WT and KI mice and analyzed by mass spectrometry (Fig. 3A). Unsupervised hierarchical clustering revealed distinct O-GlcNAc modification profiles between the two genotypes (Fig. 3B).

Differential analysis identified 116 altered O-GlcNAc-enriched proteins or modification events, of which 73 were increased and 43 were decreased in KI mice (Fig. 3C, D). Analysis of the paired total proteome identified only a small number of differentially expressed proteins, none of which overlapped with the 116 differential O-GlcNAc-enriched entries. Moreover, the abundance of their corresponding parent proteins was generally stable, suggesting that the observed differences were unlikely to be driven primarily by changes in total protein abundance.

Gene Ontology analysis showed that the differential O-GlcNAc-enriched proteins were associated with protein dephosphorylation and its regulation, ubiquitin-protein transferase activity, synaptic organization, presynaptic structures, cytoskeletal organization, and protein binding (Fig. 3E). KEGG analysis was then performed separately for relatively increased and decreased entries. Increased entries in KI mice were enriched in autophagy, Wnt signaling, oxidative phosphorylation, the tricarboxylic acid cycle, peroxisomal function, and amino acid and energy metabolism. Decreased entries were primarily associated with long-term potentiation, glutamatergic synapses, neuroactive ligand–receptor interactions, gap junctions, and cell adhesion molecules (Fig. 3F).

These findings demonstrate extensive remodeling of the O-GlcNAc-modified proteome in KI mice, involving metabolic, proteostatic, and synaptic processes

TMG improves motor and neuropathological phenotypes in MSA-KI mice

The prominent α-syn pathology, functional abnormalities, and reduced O-GlcNAcylation observed around 9 months suggested that this period might represent an important stage linking O-GlcNAc dysregulation to disease progression. We therefore treated KI mice with TMG, an OGA inhibitor, for 8 weeks beginning at 8 months of age and evaluated motor performance and brain pathology (Fig. 4A).

TMG did not significantly affect grip strength in KI mice (Fig. 4B). After 8 weeks of treatment, however, TMG-treated KI mice showed a longer rotarod latency and a shorter balance-beam traversal time than PBS-treated KI mice, indicating improved motor coordination and balance (Fig. 4C, D).

RL2 immunoblotting was used to confirm the pharmacological effect of TMG. Although RL2 levels did not differ significantly between PBS-treated WT and PBS-treated KI mice at the endpoint, TMG significantly increased global O-GlcNAcylation in both the cerebellum and basal ganglia of KI mice (Fig. 4E, G). Cerebellar immunofluorescence similarly showed lower RL2 intensity in PBS-treated KI mice than in PBS-treated WT mice and a significant increase following TMG treatment (Supplementary Fig. 4A).

TMG also reduced pS129-α-syn levels in the cerebellum and basal ganglia, whereas total α-syn levels did not differ significantly among the three groups (Fig. 4F, H). Consistent with these findings, immunofluorescence analysis showed reduced pS129-α-syn immunoreactivity in both brain regions following TMG treatment (Fig. 4I). These results indicate that increasing O-GlcNAcylation preferentially reduced pathological α-syn without altering total α-syn abundance.

TMG significantly increased TH immunoreactivity in KI mice, suggesting partial preservation of the nigrostriatal dopaminergic phenotype (Fig. 4G). In contrast, TMG did not significantly alter the number of cerebellar Calbindin-D28K-positive cells (Supplementary Fig. 4B). Finally, Iba1 and GFAP immunofluorescence intensities were significantly higher in PBS-treated KI mice than in PBS-treated WT mice, indicating microglial and astrocytic activation. Both signals were significantly reduced by TMG treatment (Fig. 4K, L), suggesting attenuation of glial reactivity.

Together, these findings show that TMG effectively increased brain O-GlcNAcylation and was associated with improved motor coordination, reduced pS129-α-syn pathology, partial restoration of TH immunoreactivity, and attenuated glial activation in MSA-KI mice.

Bidirectional modulation of O-GlcNAcylation alters α-syn pathology and cell viability

TPPP, also known as p25α, is an oligodendroglial-enriched protein and a major component of glial cytoplasmic inclusions in MSA that promotes α-syn aggregation. We therefore introduced TPPP into α-syn-expressing MO3.13 cells to better model oligodendroglial α-syn pathology. Two complementary cell

systems were established: a transient model generated by cotransfecting parental MO3.13 cells with SNCA and TPPP, and a stable model generated by transfecting TPPP into MO3.13-SNCA cells (Fig. 5A).

In the transient model, *SNCA* expression increased the pS129-α-syn/total α-syn ratio, which was further elevated by TPPP expression. TPPP overexpression similarly increased this ratio in the stable model (Fig. 5B). TPPP also enhanced granular or aggregate-like α-syn immunoreactivity and increased ThT fluorescence in both models (Fig. 5C, D). Consistently, *SNCA* expression reduced cell viability in the transient model, with a further reduction following TPPP coexpression, whereas TPPP overexpression reduced viability in the stable model (Fig. 5E). Thus, TPPP exacerbated α-syn phosphorylation, aggregation, and loss of cell viability.

Baseline alterations in the O-GlcNAc system differed between the two models. In the transient model, coexpression of *SNCA* and *TPPP* increased OGT levels without significantly altering global O-GlcNAcylation or OGA levels. In the stable model, TPPP overexpression increased global O-GlcNAcylation without affecting OGT or OGA levels (Supplementary Fig. 5B).

O-GlcNAcylation was then bidirectionally modulated using TMG and the OGT inhibitor OSMI-1 (Fig. 5F). In both models, TMG increased global O-GlcNAcylation, whereas OSMI-1 decreased it. TMG reduced the pS129-α-syn/total α-syn ratio in the stable but not the transient model, whereas this ratio was higher after OSMI-1 treatment than after TMG treatment (Fig. 5G). Thus, the effect of TMG on relative α-syn phosphorylation was model-dependent.

TMG reduced ThT fluorescence and improved cell viability in both models, whereas OSMI-1 produced the opposite effects (Fig. 5H, I). To determine whether the protective effects of TMG involved direct O-GlcNAcylation of α-syn, we performed both α-syn immunoprecipitation in mouse and FLAG-α-syn immunoprecipitation in cell. Neither approach detected a clear O-GlcNAc signal at the expected molecular weight of α-syn (Supplementary Fig. 3, 6), providing no evidence for detectable direct O-GlcNAcylation of α-syn under our experimental conditions.

These bidirectional effects support an association between increased O-GlcNAcylation and reduced protein aggregation and cellular toxicity in oligodendroglial α-syn models. However, the present findings do not support detectable direct O-GlcNAcylation of α-syn as the primary mechanism underlying the protective effects of TMG.

Discussion

In this study, we developed a novel CRISPR/Cas9-mediated knock-in mouse model of MSA in which human α-syn expression was targeted to oligodendrocytes. KI mouse model of MSA that recapitulated oligodendroglial α-syn pathology, striatonigral and olivopontocerebellar involvement, progressive motor impairment, and regional brain atrophy which is several key pathological and functional features of MSA. We further identified disease-stage-dependent disruption of brain O-GlcNAc homeostasis in KI mice, accompanied by extensive remodeling of the O-GlcNAc-modified proteome. Increasing O-GlcNAcylation,

improved selected motor phenotypes and attenuated α-syn pathology, nigrostriatal dopaminergic injury, and glial activation. Consistently, bidirectional modulation of O-GlcNAcylation altered α-syn abundance and aggregation and cell viability in an oligodendroglial cell model. Together, these findings link altered O-GlcNAc homeostasis to MSA-associated α-syn pathology and suggest that modulation of O-GlcNAcylation may represent a potential strategy for slowing pathological progression in MSA.

The formation of α-syn-rich glial cytoplasmic inclusions GCIs in oligodendrocytes is a defining pathological feature of MSA[32, 33]. How α-syn initially accumulates in oligodendrocytes remains unclear. Several mechanisms have been proposed, including α-syn expression within oligodendrocytes, intercellular transfer, impaired protein clearance, and alterations in the oligodendroglial environment. Theses changes may disrupt oligodendrocyte function and ultimately cause secondary neuronal degeneration[5, 34–37]. Targeted expression of human α-syn in oligodendrocytes therefore provides a pathologically relevant strategy for modeling MSA. In the present study, human SNCA expression is driven by oligodendrocyte-specific regulatory elements. Human α-syn was stably expressed in multiple brain regions, including the cerebellum and brainstem, and pS129 α-syn levels increased at an early stage. Because S129 phosphorylation is highly enriched in pathological α-syn inclusions, it is widely used as a marker of synucleinopathy burden[38, 39]. The oligodendroglial localization of inclusion-like pS129 α-syn signals, together with the presence of high-molecular-weight species in detergent-insoluble fractions, supports pathological α-syn aggregation in this model. Although the ultrastructural and molecular equivalence of these aggregates to mature human GCIs remains to be established, their cellular localization, phosphorylation, and detergent insolubility recapitulate key features of MSA-related α-syn pathology[40, 41].

Beyond oligodendroglial α-syn pathology, the MSA mice exhibited abnormalities involving both the striatonigral and olivopontocerebellar systems[42, 43]. SND primarily involves impairment of the nigral dopaminergic system and striatal circuitry[43]. Reduced TH immunoreactivity and MRI-detected atrophy of the striatum and substantia nigra supported nigrostriatal degeneration. Whereas reduced Calbindin-D28K, pontine volume loss, and a trend toward cerebellar atrophy indicated olivopontocerebellar involvement[44, 45]. These pathological changes were accompanied by progressive impairments in motor coordination and balance. Notably, SND-related abnormalities emerged earlier and were more pronounced than OPCA-related changes, broadly consistent with the disease course reported in previous oligodendrocyte-specific α-syn models [46–49].

Existing oligodendrocyte-specific transgenic models reproduce distinct aspects of MSA. PLP-α-syn mice develop relatively mild, progressive nigrostriatal pathology; CNP-α-syn mice exhibit prominent oligodendroglial and myelin damage without fully recapitulating the characteristic SND and OPCA patterns; and the severity of MBP–α-syn models varies markedly with transgene expression level [48–51]. Unlike these conventional transgenic lines, our model carries an oligodendrocyte-directed human SNCA expression cassette inserted at the defined H11 locus. Importantly, it combines oligodendroglial α-syn pathology with SND- and OPCA-related changes, regional brain atrophy, progressive motor impairment,

and selected autonomic abnormalities. Thus, its principal value lies in its defined knock-in design and broad, progressive MSA-like phenotype, providing a useful platform for mechanistic and preclinical studies.

After establishing the pathological and behavioral phenotypes of the MSA mice, we found that brain O-GlcNAcylation exhibited a stage-specific reduction in KI mice. Global O-GlcNAcylation was decreased in the cerebellum and basal ganglia at 9 months of age, with reduced cerebellar O-GlcNAcylation immunoreactivity providing consistent histological evidence. In contrast, no significant differences were observed at 6, 8, 12, or 20 months, suggesting that O-GlcNAcylation dysregulation may occur within a specific pathological window rather than decline progressively with age. Disruption of O-GlcNAcylation homeostasis may represent a shared pathological mechanism across several neurodegenerative disorders. Reduced O-GlcNAcylation has been associated with cognitive impairment, diminished adult neurogenesis, and enhanced gliogenesis[52, 53], and has also been reported in AD, PD, Huntington's disease, and amyotrophic lateral sclerosis[25, 54–56]. Consistent with these observations, our study is the first to identify a disease-stage-dependent reduction in O-GlcNAcylation in an MSA-like animal model, suggesting that impaired O-GlcNAc homeostasis may contribute to MSA pathogenesis.

O-GlcNAc levels are jointly controlled by OGT and OGA. In the present study, OGT protein levels were significantly reduced in the basal ganglia and cerebellum of 9-month-old KI mice, suggesting that decreased OGT expression may be an important molecular basis for deficient O-GlcNAcylation in MSA-like pathology. During normal aging, reductions in OGT expression and activity contribute to a global decline in brain protein O-GlcNAcylation[22, 57, 58]. To determine whether α-syn directly interacts with OGT, we performed co-immunoprecipitation experiments but detected no stable, specific association between the two proteins. Thus, the reduction in OGT is unlikely to result from a stable direct α-syn-OGT interaction and may instead involve α-syn-associated cellular stress that alters transcriptional regulation, protein stability, or metabolic state[59, 60]. Changes in OGT enzymatic activity, subcellular localization, and the availability of UDP-GlcNAc may further influence global O-GlcNAcylation[61].

O-GlcNAc proteomics further revealed substrate-selective changes in MSA. MSA-like pathology therefore does not appear to cause a uniform loss of O-GlcNAcylation across all proteins, but may instead remodeling this modification among functionally distinct substrates. O-GlcNAc dysregulation in MSA-like pathology may involve metabolic adaptation, neuronal signaling, and proteostasis[19, 62]. Increased modification of metabolism-related proteins may reflect an adaptive response to pathological stress, whereas decreased modification of proteins involved in synaptic and neuronal signaling is biologically consistent with the neurological dysfunction observed in the model. However, enrichment analysis identifies the functional categories of differentially modified proteins and does not, by itself, establish activation or inhibition of the corresponding pathways. The functional consequences of these changes therefore require direct validation.

The extensive remodeling of the O-GlcNAc-modified proteome, together with the global reduction in brain O-GlcNAcylation in 9-month-old KI mice, suggested that disrupted O-GlcNAc homeostasis may

contribute to MSA-like pathology. We therefore used the OGA inhibitor TMG to increase brain O-GlcNAcylation and assess its therapeutic potential. TMG reduced pS129 α-syn levels in affected brain regions without significantly altering total α-syn, suggesting a preferential reduction in pathological α-syn burden. Consistent with this effect, TMG partially restored TH immunoreactivity in the substantia nigra and improved motor performance, as evidenced by faster balance-beam traversal, prolonged rotarod latency, and a trend toward normalized stride width. These findings are consistent with previous evidence that O-GlcNAc homeostasis supports dopaminergic axons, synapses, and neuronal survival, whereas increasing O-GlcNAcylation by reducing OGA activity attenuates α-syn-associated injury[26, 27, 63].

Neuroinflammation was also prominent in MSA-KI mice, as indicated by increased Iba1 and GFAP immunoreactivity, consistent with the widespread glial activation observed in MSA[64].TMG attenuated both microglial and astrocytic reactivity, in line with studies showing that increased O-GlcNAcylation suppresses inflammatory responses in models of PD, AD, and cerebral ischemia[29, 65–68], supporting an anti-inflammatory role for enhanced O-GlcNAcylation across diverse neurological disease models. TMG also reduced Iba1 and GFAP immunoreactivity, potentially through both direct modulation of glial inflammatory signaling and indirect attenuation of α-syn-driven neuroinflammation.

In MO3.13-SNCA cells, TPPP expression alone increased global O-GlcNAcylation, but this response was insufficient to prevent α-syn phosphorylation and aggregation or loss of cell viability. This finding may reflect a compensatory O-GlcNAc response to acute proteotoxic stress. Further elevation of O-GlcNAcylation with TMG reduced α-syn abundance and aggregation and improved cell viability, whereas lowering O-GlcNAcylation with OSMI-1 produced the opposite effects. These bidirectional pharmacological findings provide additional evidence for a protective role of O-GlcNAcylation.

Previous biochemical studies have shown that site-specific O-GlcNAcylation of α-syn, including at T72 and S87, can reduce its aggregation propensity and toxicity [69–71]. In our experimental system, however, neither RL2 immunoprecipitation nor reciprocal FLAG–α-syn immunoprecipitation detected an O-GlcNAc signal corresponding to α-syn. Thus, our findings do not support a detectable increase in direct α-syn O-GlcNAcylation as the primary mechanism underlying the protective effects of TMG. Instead, the enrichment of differentially O-GlcNAcylated proteins in pathways related to metabolism, synaptic function, ubiquitination, and proteostasis raises the possibility that TMG influences α-syn pathology indirectly through broader O-GlcNAc-sensitive cellular processes. Nevertheless, because O-GlcNAc modification can be low in abundance and site occupancy, conventional immunoprecipitation may lack sufficient sensitivity to exclude direct α-syn O-GlcNAcylation completely.

This study has several limitations. First, although KI mice exhibited oligodendroglial pS129-α-syn accumulation and SND- and OPCA-related alterations, whether these inclusions fully reproduce the ultrastructural and molecular features of mature GCIs in patients with MSA remains unclear. Second, O-GlcNAc levels were assessed in cross-sectional cohorts; therefore, their longitudinal changes and the significance of the reduction observed at 9 months remain undetermined. Third, TMG globally inhibits OGA and affects numerous O-GlcNAc substrates. Its protective effects have not been validated using

genetic manipulation, site-directed mutagenesis, or rescue experiments. Thus, the key substrates and molecular mechanisms underlying O-GlcNAc-mediated regulation of α-syn homeostasis require further investigation.

Conclusion

In conclusion, we developed and characterized a PLP1-driven hSNCA KI mouse model that recapitulates key pathological and functional features of MSA. The model exhibited stage- and region-dependent disruption of O-GlcNAcylation homeostasis and extensive remodeling of the O-GlcNAc-modified proteome. Increasing O-GlcNAcylation with TMG reduced pathological α-syn accumulation and glial activation, partially restored the dopaminergic phenotype, and improved motor function. Cellular experiments further supported a protective role for O-GlcNAcylation. These findings identify O-GlcNAc dysregulation as a potentially modifiable component of MSA-like pathology and support further investigation of O-GlcNAcylation. as a therapeutic target.

Declarations

Funding

This study was funded by the National Key R&D Program of China (No. 2021YFA0805200 to H Jiang), the National Natural Science Foundation of China (U25A2058, 82571433 to H Jiang; 82571632, 82371272 to Z Chen; 82301628 to L Wan; 82401496 to L Peng), the Scientific Research Program of FuRong Laboratory(No. 2025PT5014, 2025PT5001 to H Jiang), the Natural Science Foundation of Hunan Province (No. 2024JJ3050 to H Jiang; 2025JJ20078 to Z Chen; 2024JJ6638 to L Wan; 2025JJ60489 to L Peng), The Science and Technology Innovation Program of Hunan Province(2026RC9017 to H Jiang), the Major Scientific Research Project for High-level Health Talent in Hunan Province(No.R2023047 to H Jiang), MIIT Project for Open Competition and Leadership in AI Medical Device Innovation(No.2025-AISJK-01009 to H Jiang), the Central South University Research Programme of Advanced Interdisciplinary Study (No. 2023QYJC010 to H Jiang), Central South University Clinical Research Zhang Xiao-qian Program(ZXQ2026A08 to H Jiang), Postdoctoral Fellowship Program of CPSF(GZB20230870 to L Peng), and China Postdoctoral Science Foundation (2024M753690 to L Peng).

Author Contribution

X.D, L.W, X.Y, and H.J contributed to the conception and design of the study. X.D, S.Z contributed to data collection. X.D contributed to data analysis. X.D and L.W drafted the manuscript. All authors performed the reviewing and editing of the manuscript. All authors contributed to the article and approved the submitted version.

Data Availability

The data supporting the findings of this study are available from the corresponding author upon reasonable request.

References

1. Wenning GK, Colosimo C, Geser F, Poewe W. Multiple system atrophy. Lancet Neurol. 2004;3(2):93–103.
2. Poewe W, Stankovic I, Halliday G, Meissner WG, Wenning GK, Pellecchia MT, et al. Multiple system atrophy. Nat Rev Dis Primers. 2022;8(1):56.
3. Fanciulli A, Wenning GK. Multiple-system atrophy. N Engl J Med. 2015;372(3):249–63.
4. Dong X, Chen D, Wan L, Peng L, Chen Z, Ouyang R, et al. A meta-analysis of survival and prognostic factors in multiple system atrophy. J Neurol. 2025;272(7):467.
5. Ndayisaba A, Halliday GM, Khurana V. Multiple System Atrophy: Pathology, Pathogenesis, and Path Forward. Annu Rev Pathol. 2025;20(1):245–73.
6. Low PA, Reich SG, Jankovic J, Shults CW, Stern MB, Novak P, et al. Natural history of multiple system atrophy in the USA: a prospective cohort study. Lancet Neurol. 2015;14(7):710–9.
7. Wenning GK, Geser F, Krismer F, Seppi K, Duerr S, Boesch S, et al. The natural history of multiple system atrophy: a prospective European cohort study. Lancet Neurol. 2013;12(3):264–74.
8. Grossauer A, Sidoroff V, Heim B, Seppi K. Symptomatic Care in Multiple System Atrophy: State of the Art. Cerebellum. 2023;22(3):433–46.
9. Köllensperger M, Geser F, Ndayisaba JP, Boesch S, Seppi K, Ostergaard K, et al. Presentation, diagnosis, and management of multiple system atrophy in Europe: final analysis of the European multiple system atrophy registry. Mov Disord. 2010;25(15):2604–12.
10. Papp MI, Kahn JE, Lantos PL. Glial cytoplasmic inclusions in the CNS of patients with multiple system atrophy (striatonigral degeneration, olivopontocerebellar atrophy and Shy-Drager syndrome). J Neurol Sci. 1989;94(1–3):79–100.
11. Wakabayashi K, Yoshimoto M, Tsuji S, Takahashi H. Alpha-synuclein immunoreactivity in glial cytoplasmic inclusions in multiple system atrophy. Neurosci Lett. 1998;249(2–3):180–2.
12. Deleersnijder A, Gerard M, Debyser Z, Baekelandt V. The remarkable conformational plasticity of alpha-synuclein: blessing or curse? Trends Mol Med. 2013;19(6):368–77.
13. Fusco G, De Simone A, Gopinath T, Vostrikov V, Vendruscolo M, Dobson CM, et al. Direct observation of the three regions in α-synuclein that determine its membrane-bound behaviour. Nat Commun. 2014;5:3827.
14. Zarbiv Y, Simhi-Haham D, Israeli E, Elhadi SA, Grigoletto J, Sharon R. Lysine residues at the first and second KTKEGV repeats mediate α-Synuclein binding to membrane phospholipids. Neurobiol Dis. 2014;70:90–8.
15. Mavroeidi P, Arvanitaki F, Vetsi M, Becker S, Vlachakis D, Jensen PH, et al. Autophagy mediates the clearance of oligodendroglial SNCA/alpha-synuclein and TPPP/p25A in multiple system atrophy

models. Autophagy. 2022;18(9):2104–33.
16. Pukaß K, Goldbaum O, Richter-Landsberg C. Mitochondrial impairment and oxidative stress compromise autophagosomal degradation of α-synuclein in oligodendroglial cells. J Neurochem. 2015;135(1):194–205.
17. Makioka K, Yamazaki T, Fujita Y, Takatama M, Nakazato Y, Okamoto K. Involvement of endoplasmic reticulum stress defined by activated unfolded protein response in multiple system atrophy. J Neurol Sci. 2010;297(1–2):60–5.
18. Zachara NE, O'Donnell N, Cheung WD, Mercer JJ, Marth JD, Hart GW. Dynamic O-GlcNAc modification of nucleocytoplasmic proteins in response to stress. A survival response of mammalian cells. J Biol Chem. 2004;279(29):30133–42.
19. Yang X, Qian K. Protein O-GlcNAcylation: emerging mechanisms and functions. Nat Rev Mol Cell Biol. 2017;18(7):452–65.
20. Hardivillé S, Hart GW. Nutrient regulation of signaling, transcription, and cell physiology by O-GlcNAcylation. Cell Metab. 2014;20(2):208–13.
21. Zhu Y, Liu TW, Madden Z, Yuzwa SA, Murray K, Cecioni S, et al. Post-translational O-GlcNAcylation is essential for nuclear pore integrity and maintenance of the pore selectivity filter. J Mol Cell Biol. 2016;8(1):2–16.
22. Chen L, Jiang H, Licinio J, Wu H. Brain O-GlcNAcylation: Bridging physiological functions, disease mechanisms, and therapeutic applications. Mol Psychiatry. 2025;30(6):2754–72.
23. Yuzwa SA, Vocadlo DJ. O-GlcNAc and neurodegeneration: biochemical mechanisms and potential roles in Alzheimer's disease and beyond. Chem Soc Rev. 2014;43(19):6839–58.
24. Liu F, Shi J, Tanimukai H, Gu J, Gu J, Grundke-Iqbal I, et al. Reduced O-GlcNAcylation links lower brain glucose metabolism and tau pathology in Alzheimer's disease. Brain. 2009;132(Pt 7):1820–32.
25. Park J, Ha HJ, Chung ES, Baek SH, Cho Y, Kim HK, et al. O-GlcNAcylation ameliorates the pathological manifestations of Alzheimer's disease by inhibiting necroptosis. Sci Adv. 2021;7(3).
26. Miao Y, Zhang T, Ma Z, Du H, Gu Q, Jiang M, et al. Modulation of O-GlcNAc cycling influences α-synuclein amplification, degradation, and associated neuroinflammatory pathology. Mol Neurodegener. 2025;20(1):113.
27. Kim DY, Kim SM, Cho EJ, Kwak HB, Han IO. Protective effect of increased O-GlcNAc cycling against 6-OHDA induced Parkinson's disease pathology. Cell Death Dis. 2024;15(4):287.
28. Yuzwa SA, Shan X, Macauley MS, Clark T, Skorobogatko Y, Vosseller K, et al. Increasing O-GlcNAc slows neurodegeneration and stabilizes tau against aggregation. Nat Chem Biol. 2012;8(4):393–9.
29. Zhu S, Wang N, Chen S, Zou J, Tan S. Thiamet-G ameliorates Parkinson's disease-associated cognitive impairment via increasing O-GlcNAcylation of STING in the microglia. Neurochem Int. 2025;188:106014.
30. Goedert M, Spillantini MG, Del Tredici K, Braak H. 100 years of Lewy pathology. Nat Rev Neurol. 2013;9(1):13–24.

31. Goedert M, Jakes R, Spillantini MG. The Synucleinopathies: Twenty Years On. J Parkinsons Dis. 2017;7(s1):S51-s69.
32. Wenning GK, Stankovic I, Vignatelli L, Fanciulli A, Calandra-Buonaura G, Seppi K, et al. The Movement Disorder Society Criteria for the Diagnosis of Multiple System Atrophy. Mov Disord. 2022;37(6):1131–48.
33. Virameteekul S, Revesz T, Jaunmuktane Z, Warner TT, De Pablo-Fernández E. Pathological Validation of the MDS Criteria for the Diagnosis of Multiple System Atrophy. Mov Disord. 2023;38(3):444–52.
34. Kaji S, Maki T, Ishimoto T, Yamakado H, Takahashi R. Insights into the pathogenesis of multiple system atrophy: focus on glial cytoplasmic inclusions. Transl Neurodegener. 2020;9:7.
35. Mavroeidi P, Xilouri M. Autophagy-Lysosome Pathway in Multiple System Atrophy Pathogenesis: The Best Is Yet to Come. Int J Mol Sci. 2025;26(20).
36. Arawaka S, Sato H, Sasaki A, Koyama S, Kato T. Mechanisms underlying extensive Ser129-phosphorylation in α-synuclein aggregates. Acta Neuropathol Commun. 2017;5(1):48.
37. Bukhatwa S, Zeng BY, Rose S, Jenner P. A comparison of changes in proteasomal subunit expression in the substantia nigra in Parkinson's disease, multiple system atrophy and progressive supranuclear palsy. Brain Res. 2010;1326:174–83.
38. Anderson JP, Walker DE, Goldstein JM, de Laat R, Banducci K, Caccavello RJ, et al. Phosphorylation of Ser-129 is the dominant pathological modification of alpha-synuclein in familial and sporadic Lewy body disease. J Biol Chem. 2006;281(40):29739–52.
39. Fujiwara H, Hasegawa M, Dohmae N, Kawashima A, Masliah E, Goldberg MS, et al. alpha-Synuclein is phosphorylated in synucleinopathy lesions. Nat Cell Biol. 2002;4(2):160–4.
40. Schweighauser M, Shi Y, Tarutani A, Kametani F, Murzin AG, Ghetti B, et al. Structures of α-synuclein filaments from multiple system atrophy. Nature. 2020;585(7825):464–9.
41. Tu PH, Galvin JE, Baba M, Giasson B, Tomita T, Leight S, et al. Glial cytoplasmic inclusions in white matter oligodendrocytes of multiple system atrophy brains contain insoluble alpha-synuclein. Ann Neurol. 1998;44(3):415–22.
42. Koga S, Sekiya H, Kondru N, Ross OA, Dickson DW. Neuropathology and molecular diagnosis of Synucleinopathies. Mol Neurodegener. 2021;16(1):83.
43. Ozawa T, Paviour D, Quinn NP, Josephs KA, Sangha H, Kilford L, et al. The spectrum of pathological involvement of the striatonigral and olivopontocerebellar systems in multiple system atrophy: clinicopathological correlations. Brain. 2004;127(Pt 12):2657–71.
44. Rusholt EHL, Salvesen L, Brudek T, Tesfay B, Pakkenberg B, Olesen MV. Pathological changes in the cerebellum of patients with multiple system atrophy and Parkinson's disease-a stereological study. Brain Pathol. 2020;30(3):576–88.
45. Hayakawa H, Nagai M, Kawanami A, Nakata Y, Nihira T, Ogino M, et al. Loss of DARPP-32 and calbindin in multiple system atrophy. J Neural Transm (Vienna). 2013;120(12):1689–98.

46. Yazawa I, Giasson BI, Sasaki R, Zhang B, Joyce S, Uryu K, et al. Mouse model of multiple system atrophy alpha-synuclein expression in oligodendrocytes causes glial and neuronal degeneration. Neuron. 2005;45(6):847–59.
47. Mészáros L, Riemenschneider MJ, Gassner H, Marxreiter F, von Hörsten S, Hoffmann A, et al. Human alpha-synuclein overexpressing MBP29 mice mimic functional and structural hallmarks of the cerebellar subtype of multiple system atrophy. Acta Neuropathol Commun. 2021;9(1):68.
48. Refolo V, Bez F, Polissidis A, Kuzdas-Wood D, Sturm E, Kamaratou M, et al. Progressive striatonigral degeneration in a transgenic mouse model of multiple system atrophy: translational implications for interventional therapies. Acta Neuropathol Commun. 2018;6(1):2.
49. Ubhi K, Rockenstein E, Mante M, Inglis C, Adame A, Patrick C, et al. Neurodegeneration in a transgenic mouse model of multiple system atrophy is associated with altered expression of oligodendroglial-derived neurotrophic factors. J Neurosci. 2010;30(18):6236–46.
50. Kahle PJ, Neumann M, Ozmen L, Muller V, Jacobsen H, Spooren W, et al. Hyperphosphorylation and insolubility of alpha-synuclein in transgenic mouse oligodendrocytes. EMBO Rep. 2002;3(6):583–8.
51. Shults CW, Rockenstein E, Crews L, Adame A, Mante M, Larrea G, et al. Neurological and neurodegenerative alterations in a transgenic mouse model expressing human alpha-synuclein under oligodendrocyte promoter: implications for multiple system atrophy. J Neurosci. 2005;25(46):10689–99.
52. White CW, 3rd, Fan X, Maynard JC, Wheatley EG, Bieri G, Couthouis J, et al. Age-related loss of neural stem cell O-GlcNAc promotes a glial fate switch through STAT3 activation. Proc Natl Acad Sci U S A. 2020;117(36):22214–24.
53. Wheatley EG, Albarran E, White CW, 3rd, Bieri G, Sanchez-Diaz C, Pratt K, et al. Neuronal O-GlcNAcylation Improves Cognitive Function in the Aged Mouse Brain. Curr Biol. 2019;29(20):3359-69.e4.
54. Banerjee PS, Lagerlöf O, Hart GW. Roles of O-GlcNAc in chronic diseases of aging. Mol Aspects Med. 2016;51:1–15.
55. Grima JC, Daigle JG, Arbez N, Cunningham KC, Zhang K, Ochaba J, et al. Mutant Huntingtin Disrupts the Nuclear Pore Complex. Neuron. 2017;94(1):93–107.e6.
56. Hsieh YL, Su FY, Tsai LK, Huang CC, Ko YL, Su LW, et al. NPGPx-Mediated Adaptation to Oxidative Stress Protects Motor Neurons from Degeneration in Aging by Directly Modulating O-GlcNAcase. Cell Rep. 2019;29(8):2134-43.e7.
57. Lee BE, Suh PG, Kim JI. O-GlcNAcylation in health and neurodegenerative diseases. Exp Mol Med. 2021;53(11):1674–82.
58. Wang Z, Li X, Spasojevic I, Lu L, Shen Y, Qu X, et al. Increasing O-GlcNAcylation is neuroprotective in young and aged brains after ischemic stroke. Exp Neurol. 2021;339:113646.
59. Park SK, Zhou X, Pendleton KE, Hunter OV, Kohler JJ, O'Donnell KA, et al. A Conserved Splicing Silencer Dynamically Regulates O-GlcNAc Transferase Intron Retention and O-GlcNAc Homeostasis. Cell Rep. 2017;20(5):1088–99.

60. Park S, Pak J, Jang I, Cho JW. Inhibition of mTOR affects protein stability of OGT. Biochem Biophys Res Commun. 2014;453(2):208–12.
61. Hanover JA, Krause MW, Love DC. Bittersweet memories: linking metabolism to epigenetics through O-GlcNAcylation. Nat Rev Mol Cell Biol. 2012;13(5):312–21.
62. Hart GW, Slawson C, Ramirez-Correa G, Lagerlof O. Cross talk between O-GlcNAcylation and phosphorylation: roles in signaling, transcription, and chronic disease. Annu Rev Biochem. 2011;80:825–58.
63. Lee BE, Kim HY, Kim HJ, Jeong H, Kim BG, Lee HE, et al. O-GlcNAcylation regulates dopamine neuron function, survival and degeneration in Parkinson disease. Brain. 2020;143(12):3699–716.
64. Matsuse D, Yamaguchi H, Harada M, Kira YI, Nishimura Y, Masaki K, et al. A unique microglia subset associated with aggressive α-synucleinopathy uncovered in a rapidly progressive multiple system atrophy cerebellar type model. Neurobiol Dis. 2026;218:107206.
65. Garcia ML, Denton AR, Jackson NL, Scofield MD, McMahon LL. Pharmacologically increasing O-GlcNAcylation increases complexity of astrocytes in the dentate gyrus of TgF344-AD rats. Front Aging Neurosci. 2025;17:1690410.
66. Hwang SY, Shin JH, Hwang JS, Kim SY, Shin JA, Oh ES, et al. Glucosamine exerts a neuroprotective effect via suppression of inflammation in rat brain ischemia/reperfusion injury. Glia. 2010;58(15):1881–92.
67. He Y, Ma X, Li D, Hao J. Thiamet G mediates neuroprotection in experimental stroke by modulating microglia/macrophage polarization and inhibiting NF-κB p65 signaling. J Cereb Blood Flow Metab. 2017;37(8):2938–51.
68. Wang M, Zhu W, Guo Y, Zeng H, Liu J, Liu J, et al. Astragalus polysaccharide treatment relieves cerebral ischemia–reperfusion injury by promoting M2 polarization of microglia by enhancing O-GlcNAcylation. Metab Brain Dis. 2024;40(1):16.
69. Marotta NP, Lin YH, Lewis YE, Ambroso MR, Zaro BW, Roth MT, et al. O-GlcNAc modification blocks the aggregation and toxicity of the protein α-synuclein associated with Parkinson's disease. Nat Chem. 2015;7(11):913–20.
70. Galesic A, Rakshit A, Cutolo G, Pacheco RP, Balana AT, Moon SP, et al. Comparison of N-Acetyl-Glucosamine to Other Monosaccharides Reveals Structural Differences for the Inhibition of α-Synuclein Aggregation. ACS Chem Biol. 2021;16(1):14–9.
71. Wang Z, Udeshi ND, O'Malley M, Shabanowitz J, Hunt DF, Hart GW. Enrichment and site mapping of O-linked N-acetylglucosamine by a combination of chemical/enzymatic tagging, photochemical cleavage, and electron transfer dissociation mass spectrometry. Mol Cell Proteomics. 2010;9(1):153–60.

Figures

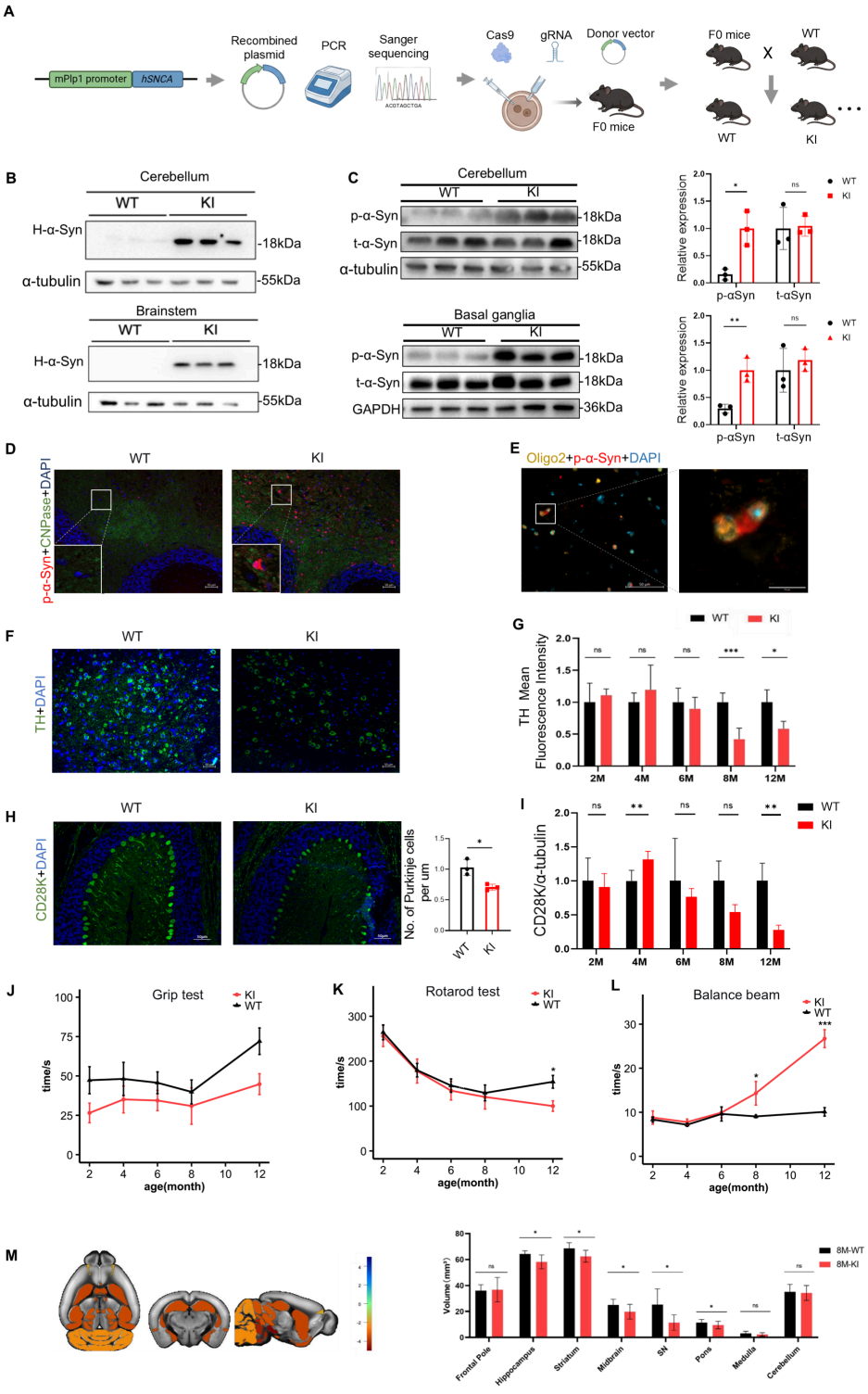


Figure 1

Generation and characterization of an oligodendroglial human α-synuclein knock-in mouse model

(A) Schematic representation of the CRISPR/Cas9-mediated strategy used to generate KI mice expressing human *SNCA*under the control of the mouse *Plp1* promoter.
(B) Representative immunoblots showing human α-syn expression in the cerebellum and brainstem of 2-

month-old WT and KI mice.
(C) Representative immunoblots and quantification of pS129-α-syn and total α-syn in the cerebellum and basal ganglia of WT and KI mice.
(D) Representative immunofluorescence images showing pS129-α-syn signals in CNPase-positive oligodendroglial regions of the cerebellum in 8-month-old mice. Scale bar, 50μm.

(E) Representative immunofluorescence images showing pS129-α-syn signals surrounding OLIG2-positive nuclei in the cerebellum of 8-month-old mice. Boxed regions are shown at higher magnification. Boxed region indicates inclusion-like cytoplasmic pS129-α-syn signals. Scale bars: 50μm in the low-magnification images and 10μm in the enlarged images.
(F, G) Representative immunofluorescence images and quantification of TH immunoreactivity in the substantia nigra of WT and KI mice at the indicated ages. Scale bar, 50μm.
(H) Representative images and quantification of cerebellar Calbindin-D28K expression and Calbindin-D28K-positive Purkinje cells. Positive cell numbers were normalized to the length of the Purkinje cell layer. Scale bar, 50μm.

(I) Representative quantification of Calbindin-D28K expression in the cerebellum of WT and KI mice at the indicated ages.
(J-L) Motor performance of male WT and KI mice assessed using the grip-strength hanging test (J), rotarod test (K), and balance-beam test (L). n=8.
(M) Representative structural magnetic resonance images and regional brain segmentation, together with quantification of brain-region volumes, in 8-month-old WT and KI mice.

Data are presented as the mean ± SEM. Each point represents an individual animal. *P<0.05, **P<0.01, ***P<0.001, and ****P<0.0001; ns, not significant.

Abbreviations: α-syn, α-synuclein; KI, knock-in; p-α-syn (pS129-α-syn), Ser129-phosphorylated α-synuclein; TH, tyrosine hydroxylase; CD28K, Calbindin-D28K; DAPI, 4',6-diamidino-2-phenylindole; WT, wild type.

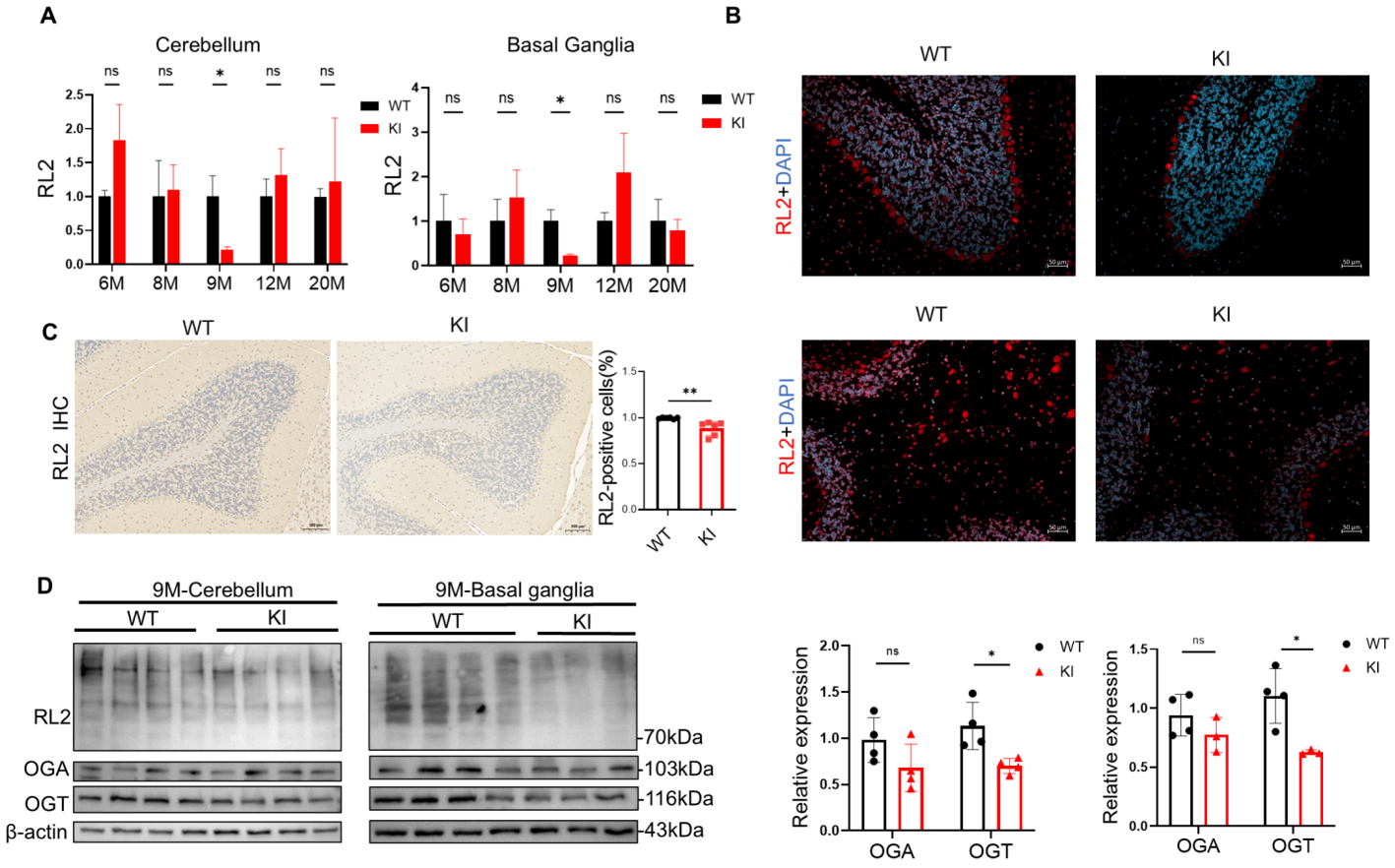


Figure 2

Stage-dependent alterations in brain O-GlcNAc homeostasis in KI mice.
(A) Quantification of global protein O-GlcNAcylation in the cerebellum and basal ganglia of WT and KI mice at the indicated ages.

(B) Representative RL2 immunofluorescence images of the cerebellum from 9-month-old WT and KI mice. The upper panels show the cerebellar lobules, and the lower panels show the cerebellar white matter. Scale bar, 50μm.

(C) Representative RL2 immunohistochemical images and quantification of the percentage of RL2-positive cells in the cerebellum lobules of 9-month-old WT and KI mice. Scale bar, 100μm.
(D) Representative immunoblots and quantification of OGA and OGT protein levels in the cerebellum and basal ganglia of 9-month-old WT and KI mice.

Data are presented as the mean±SEM. Each point represents an individual animal where shown. Sample sizes are indicated in the corresponding panels. *P<0.05 and **P < 0.01; ns, not significant.

Abbreviations: DAPI, 4',6-diamidino-2-phenylindole; KI, knock-in; OGA, O-GlcNAcase; OGT, O-GlcNAc transferase; RL2, an antibody recognizing O-GlcNAc-modified proteins; WT, wild type.

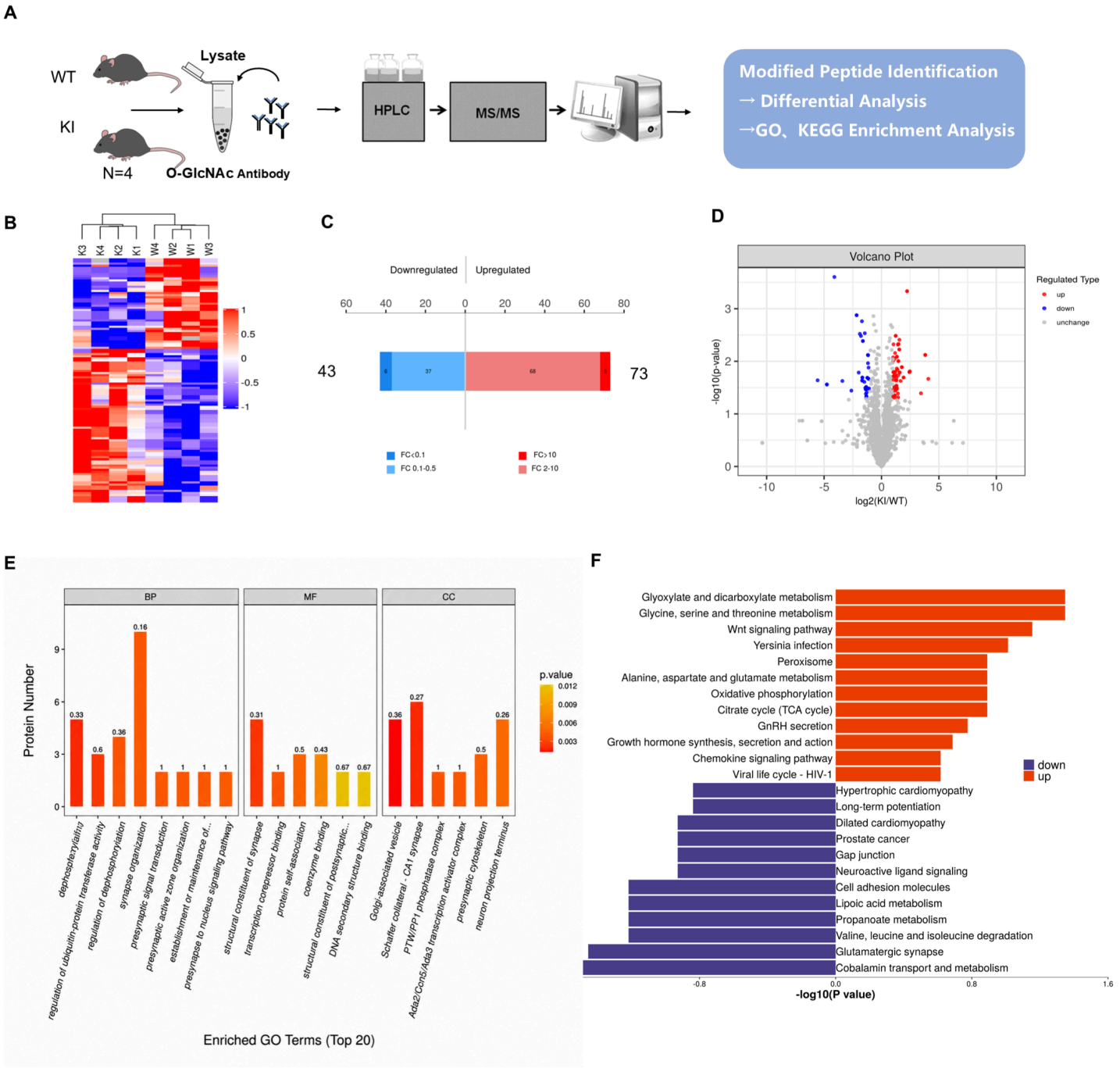


Figure 3

Remodeling of the O-GlcNAc-modified proteome in KI mice.

(A) Schematic workflow for enrichment and mass-spectrometric analysis of O-GlcNAc-modified peptides from whole-brain lysates of 12-month-old WT and KI mice (n=4 per group). Enriched peptides were analyzed by liquid chromatography-tandem mass spectrometry, followed by differential and functional enrichment analyses.

(B) Unsupervised hierarchical clustering heatmap of differentially O-GlcNAc-enriched proteins or modification events in WT and KI mice. Colors represent row-scaled relative abundance.

(C) Distribution of differentially O-GlcNAc-enriched entries according to the direction and magnitude of change. Among the 116 differential entries identified, 73 were increased and 43 were decreased in KI mice.
(D) Volcano plot showing differential O-GlcNAc-enriched entries between KI and WT mice. Red and blue dots represent relatively increased and decreased entries, respectively, and gray dots represent unchanged entries.
(E) Gene Ontology enrichment analysis of differentially O-GlcNAc-enriched proteins, categorized into biological process, molecular function, and cellular component terms. The top enriched terms are shown.
(F) KEGG pathway enrichment analysis performed separately for relatively increased and decreased O-GlcNAc-enriched entries in KI mice. Orange and purple bars represent pathways enriched among increased and decreased entries, respectively.

Abbreviations: BP, biological process; CC, cellular component; FC, fold change; GO, Gene Ontology; HPLC, high-performance liquid chromatography; KEGG, Kyoto Encyclopedia of Genes and Genomes; KI, knock-in; MF, molecular function; MS/MS, tandem mass spectrometry; WT, wild type.

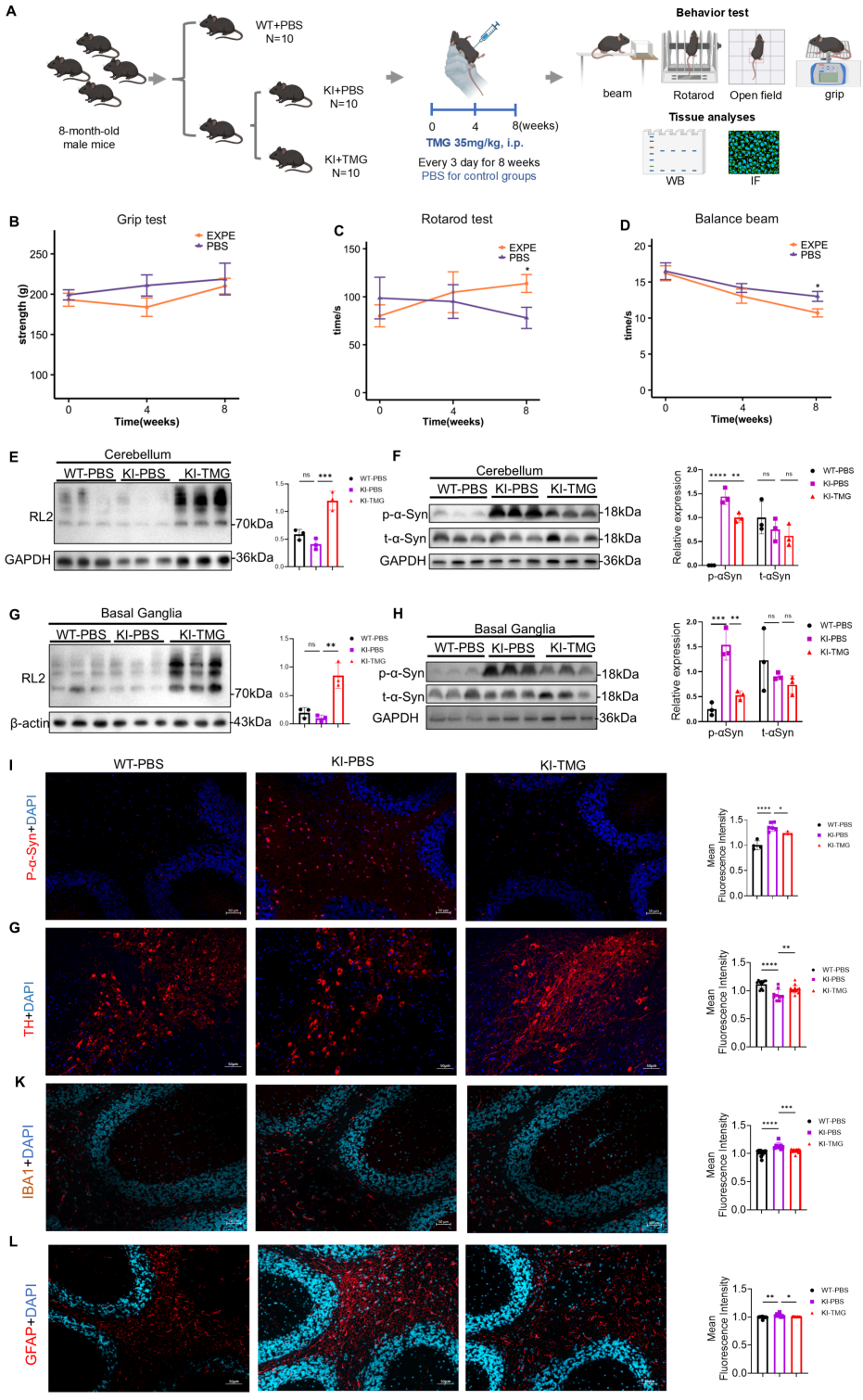


Figure 4

TMG improves motor performance and attenuates neuropathological abnormalities in MSA-KI mice. (A) Experimental design of the TMG intervention study. Eight-month-old male KI mice were treated with TMG for PBS for 8weeks. Age-matched WT mice receiving PBS were included as controls (n=10 per group).

(B-D) Motor performance of PBS-treated KI and TMG-treated KI mice assessed using the grip-strength test (B), rotarod test (C), and balance-beam test (D). n=8.
(E, G) Representative RL2 immunoblots and quantification of global protein O-GlcNAcylation in the cerebellum (E) and basal ganglia (G) of PBS-treated WT, PBS-treated KI, and TMG-treated KI mice.

(F, H) Representative immunoblots and quantification of pS129-α-syn and total α-syn in the cerebellum (F) and basal ganglia (H).
(I) Representative immunofluorescence images and quantification of pS129-α-syn immunoreactivity in the cerebellum. Scale bars, 50μm.
(J) Representative immunofluorescence images and quantification of TH immunoreactivity in the substantia nigra. Scale bars, 50μm.
(K, L) Representative immunofluorescence images and quantification of Iba1 (K) and GFAP (L) immunoreactivity in the cerebellum. Scale bars, 50μm.

Data are presented as the mean ± SEM. Each point represents an individual animal. Statistical methods are described in the Methods. *P<0.05, **P<0.01, ***P<0.001, and ****P<0.0001; ns, not significant.

Abbreviations: α-syn, α-synuclein; DAPI, 4',6-diamidino-2-phenylindole; GFAP, glial fibrillary acidic protein; Iba1, ionized calcium-binding adaptor molecule 1; KI, knock-in; p-α-syn (pS129-α-syn), Ser129-phosphorylated α-synuclein; TMG, Thiamet-G; TH, tyrosine hydroxylase; WT, wild type.

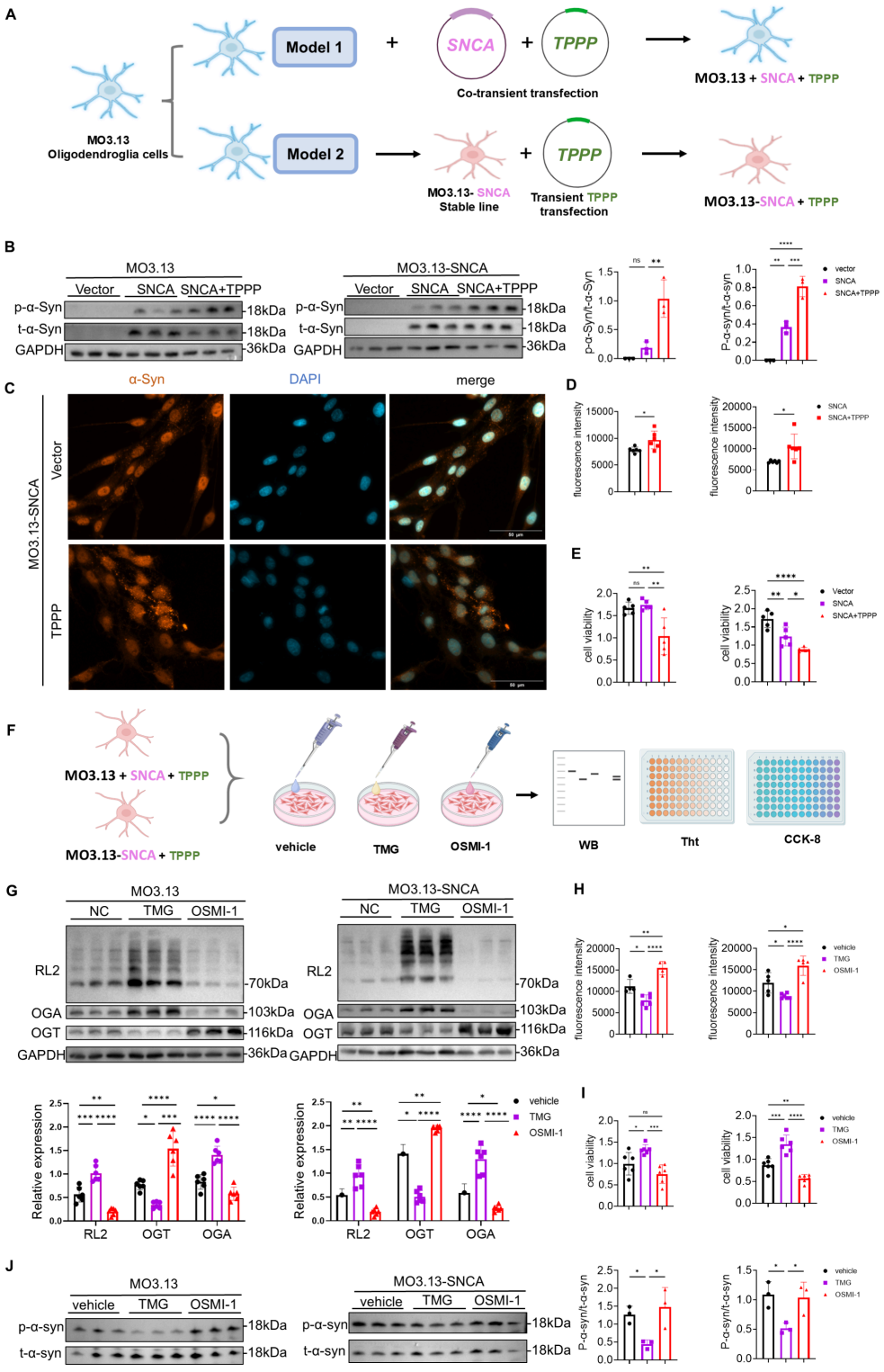


Figure 5

Bidirectional modulation of O-GlcNAcylation alters TPPP-enhanced α-syn pathology and cell viability in oligodendroglial cell models.

(A) Schematic representation of the two MO3.13 cell models.

(B) Representative immunoblots and quantification of the pS129-α-syn/total α-syn ratio in the transient and stable models.

(C) Representative immunofluorescence images showing α-syn distribution in MO3.13-SNCA cells transfected with an empty vector or a *TPPP*-expressing plasmid. TPPP overexpression increased granular or aggregate-like α-syn immunoreactivity. Scale bars, 50μm.
(D) ThT fluorescence intensity in the two cell models, reflecting the accumulation of β-sheet-rich protein aggregates.
(E) Cell viability measured using the CCK-8 assay in the two cell models.
(F) Schematic representation of the pharmacological intervention. The two cell models were treated with vehicle, TMG, or the OGT inhibitor OSMI-1

(G) Representative immunoblots and quantification of global O-GlcNAcylation, OGT, and OGA protein levels following vehicle, TMG, or OSMI-1 treatment in the two cell models.

(H) ThT fluorescence intensity following vehicle, TMG, or OSMI-1 treatment.
(I) Cell viability measured using the CCK-8 assay following vehicle, TMG, or OSMI-1 treatment.
(J) Representative immunoblots and quantification of the pS129-α-syn/total α-syn ratio following vehicle, TMG, or OSMI-1 treatment in the two cell models.

Data are presented as the mean ± SEM from independent experiments. Each point represents one independent biological replicate. **P*<0.05, ***P*<0.01, ****P*<0.001, and *****P*<0.0001; ns, not significant.

Abbreviations: α-syn, α-synuclein; p-α-syn (pS129-α-syn), Ser129-phosphorylated α-synuclein; Tht, Thioflavin T; CCK-8, Cell Counting Kit-8; DAPI, 4',6-diamidino-2-phenylindole; OGA, O-GlcNAcase; OGT, O-GlcNAc transferase; OSMI-1, O-GlcNAc transferase inhibitor-1; TMG, Thiamet-G; TPPP, tubulin polymerization-promoting protein.

Supplementary Files

This is a list of supplementary files associated with this preprint. Click to download.

- supplementarymaterial.pdf
- supplementaryoriginimages.pdf